

OPTICAL ALBEDO THEORY OF STRONGLY-IRRADIATED GIANT PLANETS: THE CASE OF HD 209458B

A. BURROWS^{1,2}, L. IBGUI² & I. HUBENY²

Submitted to Ap.J. March 17, 2008

ABSTRACT

We calculate a new suite of albedo models for close-in extrasolar giant planets and compare with the recent stringent upper limit for HD 209458b of Rowe et al. using MOST. We find that all models without scattering clouds are consistent with this optical limit. We explore the dependence on wavelength and waveband, metallicity, the degree of heat redistribution, and the possible presence of thermal inversions and find a rich diversity of behaviors. Measurements of transiting extrasolar giant planets (EGPs) at short wavelengths by MOST, Kepler, and CoRoT, as well as by proposed dedicated multi-band missions, can complement measurements in the near- and mid-IR using *Spitzer* and JWST. Collectively, such measurements can help determine metallicity, compositions, atmospheric temperatures, and the cause of thermal inversions (when they arise) for EGPs with a broad range of radii, masses, degrees of stellar insolation, and ages. With this paper, we reappraise and highlight the diagnostic potential of albedo measurements of hot EGPs shortward of $\sim 1.3 \mu\text{m}$.

Subject headings: stars: individual (HD 209458)—(stars:) planetary systems—planets and satellites: general

1. INTRODUCTION

Optical albedo measurements of solar system objects such as planets, asteroids, and moons have a strong tradition in planetary science. The associated reflectances and their wavelength dependence have been used to determine surface compositions and, in concert with infrared (IR) photometric measurements and orbital distances, can be used to determine radii. Orbital measurements can sometimes reveal masses and, given the radius, an object's average density can be calculated. This density then points to its bulk composition. In this way, optical albedo studies have often been central to constraining the interior and surface properties of solar-system bodies.

With the discovery of extrasolar giant planets (EGPs), this same program of sensing and characterization can be envisioned and numerous pilot programs to measure their optical albedos have been inaugurated (Collier-Cameron et al. 2002; Leigh et al. 2003; Leigh, Collier-Cameron, & Guillot 2003; Rowe et al. 2006). However, unless the EGP can be imaged separately from its primary star, one must contend with the severe planet–star flux ratios in the optical. At the distance of Jupiter from its primary, this ratio is $\sim 10^{-9}$. Even at the distance of the closest transiting EGPs (~ 0.05 A.U.), the optical planet–star flux ratio is around 10^{-5} (Sudarsky, Burrows, & Pinto 2000; Marley et al. 1999). These small numbers are the primary reason direct measurements in the near- to mid-infrared using *Spitzer* have been more productive of late in the study of close-in and transiting EGPs. The corresponding ratios of the absorbed optical radiation (reprocessed by the planet into the infrared) to the stellar IR (note!) can be as high as 10^{-4} to 10^{-2} . With such favorable contrasts, and using the *Spitzer* IRAC and MIPS IR photometers and the IRS spectrometer, planets outside

the solar system have been directly measured and characterized for the first time (Charbonneau et al. 2005; Deming et al. 2005,2006,2007; Harrington et al. 2006; Harrington et al. 2007; Knutson et al. 2007; Grillmair et al. 2007; Richardson et al. 2007; Swain et al. 2008). Researchers have measured atmospheric temperatures, thermal inversions, and the possible presence of water, methane and carbon monoxide. They have also discerned atmospheric features and inferred day-night climatological contrasts (Harrington et al. 2006; Knutson et al. 2007).

Nevertheless, the optical offers opportunities for measurements that can complement those in the IR to provide firmer constraints on the atmospheric properties of close-in EGPs. The albedo in the blue can reveal Rayleigh scattering off atmospheric H₂ and He to determine particle densities. Measurements in the resonance lines of the alkali metals Na ($\sim 0.589 \mu\text{m}$) and K ($\sim 0.77 \mu\text{m}$) directly test for their presence and are a counter to transit radius measurements that have already indicated the presence of Na in HD 209458b (Charbonneau et al. 2002). Importantly, albedo/reflection measurements probe different regions of the atmosphere than transit measurements.

The depth of the water feature around $\sim 0.94 \mu\text{m}$ addresses both the abundance of oxygen and of water. In these hot atmospheres, oxygen can be mostly in CO and the CO/H₂O ratio might someday provide a signature of non-equilibrium chemistry and overall metallicity. The latter addresses planetary origins and formation.

The thermal inversions recently invoked to explain the photometric reversals and flux enhancements seen in the IRAC, IRS, and/or MIPS data for HD 209458b (Hubeny, Burrows, & Sudarsky 2003; Knutson et al. 2008; Burrows et al. 2007) and for HD 149026b (Harrington et al. 2007; Burrows, Budaj, & Hubeny 2008; Fortney et al. 2006) might be due to an “extra absorber” in the optical. Such an absorber would have a strong impact on the optical reflection spectrum. If it were TiO, VO, and/or a

¹ Department of Astrophysical Sciences, Princeton University, Princeton, NJ 08544; burrows@astro.princeton.edu

² Department of Astronomy and Steward Observatory, The University of Arizona, Tucson, AZ 85721; burrows@as.arizona.edu, ibgui@as.arizona.edu, hubeny@aegis.as.arizona.edu

chemical product of photolysis, such as polyacetylenes or “tholins,” distinctive absorption features would in principle be observable³. If the temperature inversion were very strong, elevating the temperature of the upper atmosphere above the “plateau” value at depth, emission in the optical might trump absorption (Hubeny, Burrows, & Sudarsky 2003; Seager & López-Morales 2007). On the other hand, if the inversion is due not to an optical absorber, but to a mechanical heat source like the breaking of inertial or tidal waves, the resultant absence of a distinctive optical absorption feature in the albedo spectrum would be telling.

In addition, there could be thick cloud layers of silicates and/or iron. Such clouds are seen in L dwarf atmospheres and might emerge in an irradiated planet’s atmosphere when their condensation curves intersect the planet’s T/P profile. This could happen for the most severely irradiated EGPs. If these clouds form, they do so first near the sub-stellar point and equatorial regions. Reflecting clouds could increase the optical albedo by a factor of ~ 2 to ~ 5 .

Moreover, the redistribution of heat by zonal winds from the dayside to the nightside lowers the dayside temperatures and, thereby, alters the molecular composition. If we can measure this effect, parametrized by P_n ($0 < P_n < 0.5$) (Burrows et al. 2005, 2006, 2007), we might have a handle on the planet’s global climate. In the optical and very-near-IR, the variation with P_n of the planet’s flux and albedo can be a factor of 50%, depending upon wavelength. Note that the magnitude of the dependence on P_n of the planet–star flux ratio is no weaker in the optical than in the mid-IR probed by *Spitzer*.

Therefore, due to the possible features, effects, and constituents mentioned above, the monochromatic optical albedos from ~ 0.35 to $\sim 1.0 \mu\text{m}$ for the family of known transiting EGPs could vary by about an order of magnitude. Moreover, due to physical differences between the planets, the slopes of the albedo spectra at various wavelengths and the contrasts in and out of various bands can differ by many factors. The flux at the sub-stellar point (hereafter “sub-stellar flux”) on the known transiting planets ranges by \sim two orders of magnitude from $0.03 \times 10^9 \text{ ergs cm}^{-2} \text{ s}^{-1}$ for GJ 436b to $5.9 \times 10^9 \text{ ergs cm}^{-2} \text{ s}^{-1}$ for OGLE-TR-56b and the stellar types of the parents range from M, through K and G, to F. Therefore, the irradiation spectra vary substantially and this variety should translate into a variety of albedo spectra. In sum, optical albedo measurements complement near- and mid-IR measurements to more strongly constrain the physical and chemical properties of transiting EGP atmospheres than either can do alone.

Among those transiting EGPs that orbit bright and/or nearby stars, HD 189733b, HD209458b, TrES-1, HAT-P-2b, GJ 436b, XO-2b, HAT-P-1, HD149026b, and TrES-4 collectively constitute a heterogeneous class of objects that must have disparate albedo and flux signatures that will enable a fruitful photometric study of the atmospheres of close-in EGPs. For a non-transiting close-in

EGP (such as 51 Peg b, v And b, or τ Boo b), the ambiguity in the orbital inclination and radius renders interpretation more difficult, but no less interesting.

Recently, using the MOST (Microvariability & Oscillations of STars) micro-satellite (Walker et al. 2003; Matthews et al. 2004), Rowe et al. (2007) obtained a stringent $1\text{-}\sigma$ upper bound of 8.3% on the integrated optical albedo of HD 209458b⁴. The actual measurement is $3.8\% \pm 4.5\%$. More data on other transiting EGPs are sure to follow and this, along with the new HD 209458b constraint, make it a good time to address anew the theory of EGP albedos. In this paper, we compare the Rowe et al. number with a representative collection of new albedo models. Though we focus on HD 209458b, our subsidiary goal is to reignite the discussion concerning the influences on EGP albedos of variations in the physical properties of their atmospheres.

2. ALBEDO MODELS AND COMPARISON WITH THE HD 209458B DATA

The spherical albedo is the fraction of the stellar light at a given wavelength reflected into any and all angles. The Bond albedo is the frequency or wavelength integral of the spherical albedo, weighted by the incident stellar spectrum, and is a measure of the heat reflected. The Bond albedo is the quantity one uses to determine the planet’s total energy budget. However, it is the geometric albedo (A_g) that one measures when detecting the planet’s flux at the Earth. Hence, this albedo is the focus of this report and it can simply be defined using the formula:

$$F_p/F_* = A_g \left(\frac{R_p}{A} \right)^2, \quad (1)$$

where F_p/F_* is the planet–star flux ratio at full face, which for transiting planets is at secondary eclipse, R_p is the planet radius, and A is the semi-major axis of the planet’s orbit, assumed hereafter to be circular. Of course, the planet–star flux ratio varies with phase angle via the phase function (Burrows, Sudarsky, & Hubeny 2004; Sudarsky, Burrows, & Hubeny 2005), but at superior conjunction the phase function is set to one, thereby fixing the definition of A_g . Henceforth, we will not be concerned with the phase dependence and will focus on the full-face quantities A_g and F_p/F_* and their wavelength dependence.

Implicitly, the definition in eq. (1) acknowledges that at the high atmospheric temperatures of close-in planets the planet itself can be self-luminous in the near- and mid-IR and that A_g at these wavelengths can exceed one. This possibility is not at all anomalous, since in determining an albedo one is taking the ratio of planet flux to stellar flux, at the same wavelength. In the IR, the planet’s flux may be due more to the absorption and re-emission of the star’s optical flux than to its IR flux and when the star’s IR flux is the divisor (as in eq. 1), the resulting A_g can easily exceed one without violating energy conservation. Hence, the anomaly, if anomaly there is, is merely one of expectations colored by solar-system experience, for which the bodies in question are much cooler than the Sun and the concept of optical albedo is sensibly tied to reflection. However, for close-in EGPs, the fluxes

³ Note that Jupiter’s albedo spectrum in the blue is lowered by about a factor of two shortward of $\sim 0.5 \mu\text{m}$ due to the presence of non-equilibrium upper-atmosphere absorbing species of unknown origin.

⁴ Rowe et al. achieve a photometric accuracy better than 10^{-5} .

are more and more thermal longward of $\sim 0.7 \mu\text{m}$. Nevertheless, incorporating the stellar flux as a boundary condition and solving the equations of radiative transfer for all wavelengths self-consistently, yields values of F_p/F_* , from which A_g as a function of wavelength can be derived using eq. (1).

To produce our models for F_p/F_* and A_g , we employ the self-consistent atmosphere code and solution techniques described in Hubeny & Lanz (1995), Burrows, Hubeny, & Sudarsky (2005), Burrows, Sudarsky, & Hubeny (2006), and Burrows, Budaj, & Hubeny (2008), to which the reader is referred for details. In Burrows, Budaj, & Hubeny (2008), we also describe how we now handle heat redistribution for a given P_n and how we derive the flux at secondary eclipse. In Sharp & Burrows (2007), we review our opacity libraries and chemical abundance calculations. The latter are done in the context of chemical equilibrium. Using these tools and databases, we have generated spectral models for HD 209458b at superior conjunction as a function of metallicity and P_n . We have also explored the dependence on a possible high-altitude “extra absorber” in the optical, as inferred for HD 209458b by Burrows et al. (2007) using the IRAC data of Knutson et al. (2008). Though the models range from $0.3 \mu\text{m}$ to $300 \mu\text{m}$, we highlight in this paper only the results shortward of $1.3 \mu\text{m}$.

Figure 1 portrays the albedo spectra for a variety of atmospheric models for HD 209458b. Superposed are the Rowe et al. (2007) upper limit ($8.3\% [1-\sigma] \equiv 3.8\% \pm 4.5\%$), the MOST transmission curve, and the model bandpass-averaged albedos. Table 1 depicts these averaged albedos, as well as the corresponding numbers for a few models of HD 189733b for comparison. The model spectra are calculated for a given triplet of P_n (0.1, 0.3, or 0.5), atmospheric metallicity (either solar or $10\times$ solar), and κ_e (0.0 or $0.1 \text{ cm}^2/g$). κ_e is the opacity of a putative extra absorber which might be necessary to generate the thermal inversion at altitude inferred from the IRAC data for HD 209458b (Knutson et al. 2008). We distribute this absorber everywhere in the atmosphere at pressures lower than ~ 0.014 bars and in the wavelength interval $0.43 \mu\text{m} < \lambda < 1.0 \mu\text{m}$. This prescription should be viewed as useful, but simplistic. To fit the HD209458b data, Burrows et al. (2007) employed a constant value of $\kappa_e = 0.1 \text{ cm}^2/g$.

Figure 1 incorporates our major results and manifests a number of features. The general trend is that the albedo decreases to shorter wavelengths until Rayleigh scattering off H_2 and He reverses this. This can occur near $\sim 0.5 \mu\text{m}$ and can be responsible for an increase in A_g of as much as an order of magnitude from $0.55 \mu\text{m}$ to $\sim 0.30 \mu\text{m}$. At its trough, A_g can be as low as (or lower than) $\sim 1\%$, but without an extra broad-band absorber as we have modeled it here it is only in the relatively narrow alkali metal features that A_g is severely low. Otherwise, the trough is around $\sim 1\%$ to $\sim 5\%$. However, this can correspond to values of F_p/F_* less than 10^{-5} and such numbers may be inaccessible from the ground for the foreseeable future. However, due to the high temperatures ($\sim 1500\text{--}2000 \text{ K}$) in HD 209458b’s atmosphere (Burrows, Budaj, & Hubeny 2007), A_g exceeds 1.0 longward of $\sim 1.0 \mu\text{m}$ to $\sim 1.1 \mu\text{m}$. In fact, using the strict definition in eq. (1), in the mid-IR A_g exceeds

10. Note that for most of our models longward of $\sim 0.7 \mu\text{m}$ A_g is above 0.1 (10%). At $\sim 1.0 \mu\text{m}$, it can be near $\sim 60\%$. Therefore, longward and shortward of the V and R bands, in the U , B , Z , Y , and z' bands, A_g can be respectable, even high. Such high values may explain the very tentative $1-\sigma$ lower limit to A_g in the B band of ~ 0.14 estimated by Berdyugina et al. (2007) for HD 189733b (see also Table 1).

However, when integrating over the MOST passband, our models, for the variety of values of P_n and metallicity, have low predicted average albedos, varying from ~ 0.017 to ~ 0.07 (Table 1). These are quite “black.” In fact, all our models are consistent with the low Rowe et al. $1-\sigma$ upper limit of 8.3%. Reflecting clouds in the atmospheres of solar-system bodies, and in previous theoretical EGP models with clouds (e.g., Sudarsky, Burrows, & Pinto 2000), have values of A_g above 0.2 (20%), usually near $\sim 30\text{--}40\%$. Such numbers are inconsistent with the Rowe et al. measurement. Therefore, a straightforward conclusion is that there are no reflecting clouds in the atmosphere of HD 209458b. Thin hazes are possible, but we estimate their optical depth in the MOST bandpass can be no larger than ~ 0.1 for high single-scattering albedos ($\Sigma = \kappa_s/(\kappa_s + \kappa_a)$). This conclusion may challenge some otherwise reasonable solutions (Fortney et al. 2003) to the anomaly in the magnitude of the transit radius in the Na-D lines measured by Charbonneau et al. (2002).

The Rowe et al. (2007) data provide only one number and the MOST transmission curve is very broad. As a result, we can derive little from these data about the atmosphere of HD 209458b. However, the variety of models depicted in Fig. 1 and Table 1 allow us to make general predictions concerning the diagnostic potential of future albedo spectrum measurements from $\sim 0.3 \mu\text{m}$ to $1.3 \mu\text{m}$ and to discuss the dependence of A_g on the physical attributes of the atmospheres of close-in EGPs.

The relative behavior in Fig. 1 of the solar metallicity models at $\kappa_e = 0$ (black and two shades of gray) as a function of P_n demonstrates that small values of P_n , which yield the hottest dayside temperatures, result in higher values of A_g longward of $\sim 0.65 \mu\text{m}$. A_g and F_p/F_* increase by $\sim 30\text{--}50\%$ as P_n shifts from 0.5 to 0.1. This is as expected, given the thermal character of the longer-wavelength fluxes. However, hotter atmospheric temperatures result in higher absorption opacities. At the shorter wavelengths, where Rayleigh scattering is manifest, these higher absorption opacities translate into lower scattering albedos. As Sudarsky, Burrows, and Pinto (2000) and van de Hulst (1974) showed, A_g decreases quickly with decreasing single-scattering albedo, as much as a factor of two for a $\sim 10\%$ decrease in Σ . We see this behavior in Fig. 1 between 0.4 and $0.5 \mu\text{m}$, where the black curve ($P_n = 0.1$) is almost a factor of two lower than the light gray curve ($P_n = 0.5$), even though the MOST averages are comparable. Hence, higher values of the heat redistribution parameter result in higher (lower) values of A_g at short (long) wavelengths.

Comparing the brown curve ($10\times$ solar, $P_n = 0.3$) with the dark gray curve (solar, $P_n = 0.3$) allows one to gauge the metallicity dependence. However, shortward of $\sim 1.3 \mu\text{m}$, the metallicity effect can be subtle. At wavelengths longer than $\sim 0.9 \mu\text{m}$, higher metallicity results in slightly lower A_g and F_p/F_* , but only by $\sim 10\%$. Between $\sim 0.85 \mu\text{m}$ and $\sim 0.55 \mu\text{m}$, the A_g s are very similar. However,

below $\sim 0.5 \mu\text{m}$, A_g s are much lower for $10\times$ solar metallicity. The higher metallicity results in much higher absorption cross sections and, hence, lower Σ . In a spectral region where Rayleigh scattering, not thermal emission, is important, as described above this translates into a much lower value of A_g . This fact is demonstrated in Table 1 by comparing the B band albedos.

Note that the transmission curves of MOST, Kepler (Borucki et al. 2003; Koch et al. 2004; D. Koch, private communication), and CoRoT⁵ penetrate progressively more and more into the red. For MOST, the wavelength on the red side at which transmission is 10% of peak is $\sim 0.75 \mu\text{m}$, for Kepler it is $\sim 0.9 \mu\text{m}$, and for CoRoT it is $\sim 1.0 \mu\text{m}$. As indicated in Table 1, the different predicted albedos for these different satellites may be crudely diagnostic of the wavelength dependence of individual models, with CoRoT sampling the longer wavelengths at which A_g is generally higher. Short of spectral measurements or multi-band photometry, a comparison of the broad-band albedos measured by these different platforms may be our only near-term means to obtain “spectral” information.

Water absorption features reside at $\sim 0.92\text{--}1.0 \mu\text{m}$ and $\sim 1.1\text{--}1.2 \mu\text{m}$ and are clearly seen in Fig. 1. Their depths can be from $\sim 50\%$ to a factor of two and are clear signatures of water’s presence. Nearly saturated, the metallicity and abundance dependence is modest, with the $10\times$ solar model lower by $\sim 20\text{--}40\%$ than the solar model. Hence, measurements in and out of these features and of the absolute A_g s would identify water’s presence and might constrain its abundance.

The red (solar) and green ($10\times$ solar) curves in Fig. 1 depict two realizations of a model with an “extra absorber” ($\kappa_e = 0.1 \text{ cm}^2/\text{g}$) in the optical that creates a thermal inversion at altitude and explains the the IRAC, MIPS, and IRS data for HD 209458b (Burrows et al. 2007). While in the mid-IR these two models differ little ($\sim 20\%$), the presence of a broad optical absorption feature can severely suppress flux where it operates. At solar metallicity (red), the effect on A_g is severe between its artificial blue ($0.43 \mu\text{m}$) and red ($1.0 \mu\text{m}$) edges. However, if the metallicity is as high as $10\times$ solar, the suppressive effect of adding an extra absorber with a given opacity is less (green curve). While at high metallicity the flux is generally lower in the optical than for all the models without inversions, it is a factor of $\lesssim 2$ times higher than for solar-metallicity models (red curve). This inverse dependence on metallicity is encouraging as a diagnostic, until one realizes that in an absolute sense the geometric albedos and flux ratios are quite low. In addition, our models place the extra absorber at the same pressure levels ($\lesssim 0.014$ bars), independent of metallicity, and, depending upon the origin of the absorber, it is likely that its physical extent will somehow be metallicity-dependent. Nevertheless, a metallicity dependence may be a future signature of the metallicity/extra-absorber combination that is not so manifest at infrared wavelengths. Clearly, knowledge of the specific absorption spectrum of the extra absorber, if it exists, would make our predictions more specific. Such would be the case if it were TiO and/or VO (Hubeny

et al. 2003). However, the cold-trap effect (Burrows et al. 2008) suggests that TiO and VO might not have the requisite abundance at altitude to explain the inversion inferred from the HD 209458b IRAC data of Knutson et al. (2008). This is an open question.

There are two final features to note concerning the models with an “extra absorber” portrayed in Fig. 1. The first is that at the shortest wavelengths the solar model has higher values of A_g (red curve). These higher albedos are a consequence of the fact that while the extra absorber heats the atmosphere at low pressures (< 0.014 bars), it results in lower temperatures for the high-pressure plateau (Burrows, Budaj, & Hubeny 2008, their Figure 1). This is near where the far-blue and near-UV photospheres reside. Lower temperatures result in lower absorptive opacities and, hence, higher scattering albedos. The result is the counter-intuitive enhancement in the albedos at the shortest wavelengths. This is less the case for the $10\times$ solar model, due to the correspondingly higher absorptive opacity. The second feature is that the model with an extra absorber that fits the HD 209458b IRAC data (Burrows et al. 2007) predicts mid-optical albedos and corresponding planet–star flux ratios that are lower, not higher, than without the absorber, mildly at odds with the suggestion of Fortney et al. (2007). This is because in these extra-absorber models the optical photosphere is at lower temperatures (and pressures) than is the temperature plateau at depth, near where the optical photosphere would reside without the extra optical absorber. The upshot is a cooler emitting surface at optical wavelengths with the extra absorber, than without, at least for the Burrows et al. (2007) models that currently fit the HD 209458b IRAC data. Of course, a more precise spectral model for the thermal inversion may lead to a different conclusion, depending on the resultant T/P profile. In addition, the much hotter upper atmospheres expected for OGLE-TR-56b, TrES-4, OGLE-TR-132b, and XO-3b may indeed manifest this albedo enhancement (Hubeny, Burrows, & Sudarsky 2003; Seager & López-Morales 2007). However, our results stress caution in making qualitative predictions for planets with thermal inversions for the planet–star flux ratios in the optical.

Moreover, if the thermal inversion is due to the breaking of mechanical waves, and not an upper atmosphere absorber in the optical, the albedo predictions could be very different. In particular, A_g in the mid-optical could be a factor of $\sim 5\text{--}10$ higher if the inversion is not due to an extra absorber. This difference might be a diagnostic of the wave breaking mechanism in planet atmospheres for which the near- and mid-IR data demand a thermal inversion.

3. SUMMARY

Focussing on HD 209458b, we have generated a new suite of albedo models for close-in extrasolar giant planets. We find that all models without scattering clouds fit the Rowe et al. (2007) albedo limit for HD 209458b and that it is no surprise that the albedo in the MOST bandpass is very low. We have explored the effects of metallicity, of the degree of heat redistribution, and of enhanced optical opacities at altitude that might create thermal inversions such as are inferred from the IRAC data for HD 209458b and HD 149026b. Measurements

⁵ The transmission curve for CoRoT can be found at <http://corotsol.obspm.fr/web-instrument/payload.param/>.

of hot EGPs at short wavelengths can complement measurements in the near- and mid-IR using *Spitzer* and JWST to determine metallicity, water abundances, atmospheric temperatures, and the cause of thermal inversions, when they arise. Moreover, albedos at short wavelengths are strongly affected by Rayleigh scattering off molecular hydrogen and helium and their measurement can be used to determine or constrain the sum of their number densities. Soon, Kepler and CoRoT will measure in slightly different wavebands the optical transits, the light curves, and the albedos of a large number of known and presently unknown transiting EGPs, thereby providing a wealth of new data and crude spectral diagnostics below $\sim 1.0 \mu\text{m}$. These data can be compared with models calculated using the formalism we applied here for HD 209458b to constrain atmospheric parameters of close-in giants with a broad range of gravities, degrees of stellar insolation, abundances, and ages. Fur-

thermore, a number of satellites dedicated to albedo measurements of dozens of close-in EGPs in several bands are being proposed. With this paper, we hope to reignite the discussion concerning EGP albedos and their diagnostic potential.

We thank Jamie Matthews, Jason Rowe, Heather Knutson, Dave Charbonneau, Bill Hubbard, Peter Goldreich, and Drew Milsom for helpful discussions and guidance and Dave Koch and the Kepler team for providing us with an electronic version of the Kepler transmission curve. This study was supported in part by NASA grants NNG04GL22G, NNX07AG80G, and NNG05GG05G and through the NASA Astrobiology Institute under Cooperative Agreement No. CAN-02-OSS-02 issued through the Office of Space Science.

REFERENCES

- Berdyugina, S.V., Berdyugin, A.V., Fluri, D.M., & Pirola, V. 2007, accepted to ApJ, arXiv:0712.0193
- Borucki, W. et al. 2003, Future EUV/UV and Visible Space Astrophysics Missions and Instrumentation. Edited by J. Chris Blades, Oswald H. W. Siegmund. Proceedings of the SPIE, Volume 4854, pp. 129-140 (2003)
- Burrows, A., Sudarsky, D., & Hubeny, I. 2004 ApJ, 609, 407
- Burrows, A., Hubeny, I., & Sudarsky, D., 2005 ApJ, 625, L135
- Burrows, A., Sudarsky, D. & Hubeny, I. 2006, ApJ, 650, 1140
- Burrows, A., Hubeny, I., Budaj, J., Knutson, H.A., & Charbonneau, D. 2007, ApJ, 668, L171
- Burrows, A., Budaj, J., & Hubeny, I. 2008, accepted to ApJ(arXiv:0709.4080).
- Charbonneau, D., Brown, T. M., Noyes, R. W., & Gilliland, R. L. 2002, ApJ, 568, 377
- Charbonneau, D. et al. 2005, ApJ, 626, 523
- Collier-Cameron, A., Horne, K., Penny, A., & Leigh, C. 2002, MNRAS, 339, 187
- Deming, D., Seager, S., Richardson, L.J., & Harrington, J., 2005, Nature, 434, 740
- Deming, D., Harrington, J., Seager, S., Richardson, L.R. 2006, ApJ, 644, 560
- Deming, D., Harrington, J., Laughlin, G., Seager, S., Navarro, S.B., Bowman, W.C., & Horning, K. 2007, submitted to ApJ Letters (arXiv:0707.2778)
- Fortney, J.J., Sudarsky, D., Hubeny, I., Cooper, C.S., Hubbard, W.B., Burrows, A., & Lunine, J.I. 2003, ApJ, 589, 615
- Fortney, J.J., Saumon, D., Marley, M.S., Lodders, K., & Freedman, R.S. 2006, ApJ, 642, 495
- Fortney, J.J., Marley, M.S., Lodders, K., & Freedman, R.S. 2007, submitted to ApJ(arXiv:0710.2558)
- Grillmair, C.J., Charbonneau, D., Burrows, A., Armus, L., Stauffer, J., Meadows, V., Van Cleve, J., & Levine, D. 2007, ApJ, 658, L115
- Harrington, J., Hansen, B., Luszcz, S., Seager, S., Deming, D., Menou, K., Cho, J., & Richardson, L. 2006, Science, 314, 623
- Harrington, J., Luszcz, S., Seager, S., Deming, D., & Richardson, L.J. 2007, Nature, 447, 691
- Hubeny, I. & Lanz, T. 1995, ApJ, 439, 875
- Hubeny, I., Burrows, A., & Sudarsky, D. 2003, ApJ, 594, 1011
- Knutson, H., Charbonneau, D., Allen, L.E., Fortney, J.J., Agol, E., Cowan, N.B., Showman, A.P., Cooper, C.S., & Megeath, S.T. 2007, Nature, 447, 183
- Knutson, H.A., Charbonneau, D., Allen, L.E., Torres, G., Burrows, A., & Megeath, S.T. 2008, ApJ, 673, 526
- Koch, D.G. et al. 2004, Optical, Infrared, and Millimeter Space Telescopes. Edited by Mather, J.C. Proceedings of the SPIE, Volume 5487, pp. 1491-1500
- Leigh, C., Collier-Cameron, A., Horne, K., Penny, A., & James, D. 2003, MNRAS, 344, 1271
- Leigh, C., Collier-Cameron, A., & Guillot, T. 2003, MNRAS, 346, 890
- Marley, M.S., Gelino, C., Stephens, D., Lunine, J.I., & Freedman, R. 1999, ApJ, 513, 879
- Matthews, J.M., Kusching, R., Guenther, D.B., Walker, G.A.H., Moffat, A.F.J., Rucinski, S.M., Sasselov, D., & Weiss, W.W. 2004, Nature, 430, 51
- Richardson, L.J., Deming, D., Horning, K., Seager, S., & Harrington, J. 2007, Nature, 445, 892
- Rowe, J.F., Matthews, J.M., Seager, S., Kuschnig, R., Guenther, D.B., Moffat, A.F.J., Rucinski, S.M., Sasselov, D., Walker, G.A.H., & Weiss, W.W. 2006, ApJ, 645, 1241
- Rowe, J.F., et al. 2007, submitted to ApJ(arXiv:0711.4111)
- Seager, S. & López-Morales, M. 2007, ApJ, 667, L191
- Sharp, C.M. & Burrows, A. 2007, ApJS, 168, 140
- Sudarsky, D., Burrows, A., & Pinto, P. 2000, ApJ, 538, 885
- Sudarsky, D., Burrows, A., Hubeny, I., & Li, A. 2005, ApJ, 627, 520
- Swain, M., Bouwman, J., Akeson, R., Lawler, S. & Beichman, C. 2008, ApJ, 674, 482 (arXiv:astro-ph/0702593)
- van de Hulst, H.C. 1974, A&A, 35, 209

TABLE 1
BAND-AVERAGED GEOMETRIC ALBEDOS FOR HD 209458B AND HD 189733B¹

Planet	Filter	MOST			Kepler			CoRoT			B Bessel			
		$\kappa_e \setminus P_n =$	0.1	0.3	0.5	0.1	0.3	0.5	0.1	0.3	0.5	0.1	0.3	0.5
HD 209458b	solar	0.0	0.070	0.066	0.063	0.111	0.095	0.079	0.136	0.117	0.097	0.077	0.085	0.0
		0.1	...	0.023	0.014	0.026	0.057	...
	10×solar	0.0	...	0.030	0.076	0.092	0.012	...
HD 189733b	solar	0.0	0.044	0.044	0.048	0.047	0.045	0.044	0.063	0.059	0.058	0.084	0.088	0.1
		0.1	...	0.022	0.007	0.017	0.073	...
	10×solar	0.0
		0.1

^aTheoretical average geometric albedos in the MOST, Kepler, CoRoT, and B (Bessell) transmission bands for various of the HD 209458b models depicted in Fig. 1, as well as for HD 189733b for comparison. For the HD 189733b model with $\kappa_e = 0.1 \text{ cm}^2/\text{g}$, we also place the extra absorber in the atmosphere below pressures of ~ 0.014 bars. Each band-averaged albedo is derived by multiplying the theoretical wavelength-dependent albedos by the corresponding normalized transmission function and then integrating over wavelength. This table summarizes the metallicity, P_n , and κ_e dependences we derive in this study. See the text for a discussion and Fig. 1.

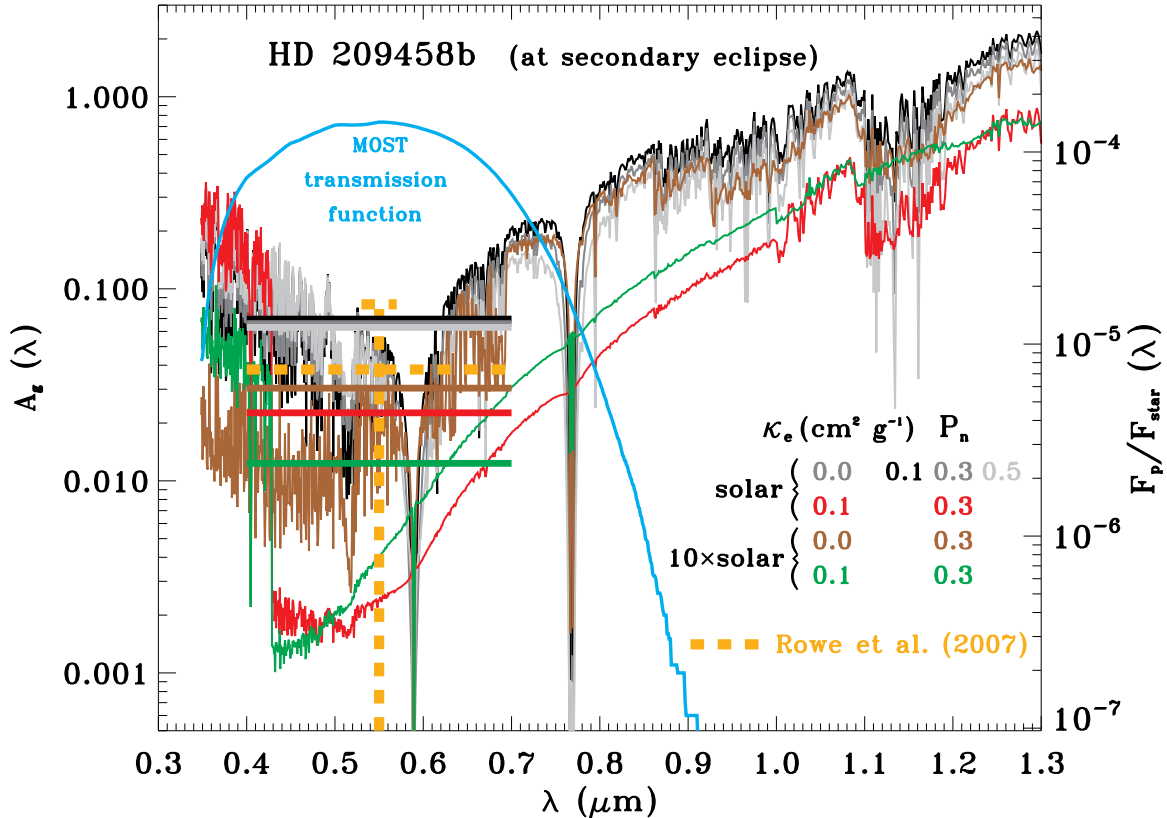


FIG. 1.— The logarithm base 10 of theoretical albedos (left axis) and F_p/F_* ratios (right axis) as a function of wavelength (in microns) from $0.35 \mu\text{m}$ to $1.3 \mu\text{m}$ for a collection of models for HD 209458b. Here $F_{\text{star}} = F_*$. Each model spectrum is for a given representative combination of P_n (either 0.1, 0.3, or 0.5), atmospheric metallicity (either solar or $10\times$ solar), and “extra absorber” opacity (κ_e , either 0.0 or $0.1 \text{ cm}^2/\text{g}$). The legend at the bottom right provides the matrix of models and the colors of the corresponding lines. The prescription for incorporating the extra absorber, when present, is described in Burrows, Budaj, & Hubeny (2008). κ_e is a phenomenological parameter with which to numerically generate a thermal inversion at low pressures. Such an inversion is inferred for HD 209458b by Burrows et al. (2007) from an analysis of its IRAC data (Knutson et al. 2008) and may be due to photolytic products, TiO/VO, or some other origin. Superposed in blue is the MOST transmission function. Since its transmission function is so broad, ranging from $\sim 0.35 \mu\text{m}$ to $0.8 \mu\text{m}$, we provide with horizontal lines the corresponding predicted average albedos as they would be measured by MOST. The Rowe et al. (2007) data ($3.8\% \pm 4.5\%$) are superposed in orange (dashed), with the topmost extent indicating the $1-\sigma$ upper limit (8.3%). See the text for a discussion of the models and their implications.